Appl. Phys. B 78, 457–463 (2004)
DOI: 10.1007/s00340-003-1373-6

Applied Physics B
Lasers and Optics

J.-J. ZONDY[1,✉]
V. VEDENYAPINE[2]
T. KAING[1]
D. LEE[1]
A. YELISSEYEV[2]
L. ISAENKO[2]
S. LOBANOV[2]

Doppler spectroscopy of NH_3 and SF_6 in the 10-μm range with a tunable $AgGaS_2$ difference-frequency spectrometer

[1] BNM-SYRTE, Observatoire de Paris (UMR-CNRS 8630), 61 Avenue de l'Observatoire, 75014 Paris, France
[2] Institute of Mineralogy and Petrography, Siberian Branch of Russian Academy of Sciences, 3 Acad. Koptyug Avenue, 630090 Novosibirsk, Russia

Received: 4 August 2003/Revised version: 31 October 2003
Published online: 19 January 2004 •

ABSTRACT A continuous-wave mid-IR diode-laser-based, dual-cavity difference-frequency spectrometer employing silver thiogallate ($AgGaS_2$) as the down-conversion material, and producing only 30 nW of usable mid-IR output, is used to record Doppler spectra of NH_3 and SF_6 around 10.2 μm and 10.5 μm over the 90-GHz range. The tuning procedure of the spectrometer as well as a baseline noise cancellation technique based on analogue signal ratioing are described. The device can potentially be used for ultra-high-resolution saturation spectroscopy, pending an improvement of the down-conversion efficiency to 1-μW power.

PACS 42.65.Ky; 42.62.Fi; 42.70.Mp; 42.72.Ai; 42.60.Da; 33.20.Ea

1 Introduction

The 9- to 12-μm mid-IR range is a target region of the electromagnetic spectrum that lacks convenient coherent radiation sources for the spectroscopic investigation of heavy spherical molecules such as NH_4, SF_6 or OsO_4. Historically, the high-power CO_2 laser was the first coherent source used for such investigations [1, 2]; however, its discontinuous tunability (typical continuous tuning range of 100 MHz spaced by 30-GHz line spacing for a low-pressure laser) restricted its use to saturation or time-resolved spectroscopy when a coincidence occurs between a lasing CO_2 isotope transition [3] and the target molecular transition. The recent advent of quantum-cascade semiconductor lasers [4, 5] that has rendered obsolete the previous cryogenically cooled Pb : salt diode lasers can offer an alternative in the deep mid IR, but their continuous-wave (cw) operation still requires cooling far below melting-ice temperature [6] and their tuning range and spectral line width remain limited. The only versatile, widely tunable sources for high-resolution spectroscopic applications in the deep mid IR rely on $\chi^{(2)}$ down-conversion processes, namely optical parametric oscillation (OPO) or difference-frequency generation (DFG), which provide the narrowest line widths in cw operation.

Because cw mid-IR OPOs generating output wavelengths above 5 microns have never been demonstrated to date, due to the lack of extremely low-loss mid-IR non-linear materials, cw DFG pumped by near-IR solid-state [7, 8] or semiconductor [9–12] lasers remains the only alternative to produce narrow-line-width deep mid-IR tunable radiation from the μW (solid-state laser) to the nW (diode-laser) power level ranges. For most molecular species, a μW-range power level is adequate for saturation spectroscopy due to the large dipole moment of IR transitions [13, 14] and to the higher detectivity of mid-IR photosensors. However, to date only very few works were devoted to cw DFG spectrometers for wavelengths longer than 10 μm [8, 10, 15, 16], a region where the use of pulsed distributed feedback quantum-cascade lasers for environmental trace-gas sensing, such as NH_3, has recently been reported [17]. In most of these cw long-wavelength generating setups (with mid-IR power level of a few to 20 nW for typical near-IR pump powers of about 300 mW), gallium selenide (GaSe) was preferred to $AgGaS_2$ owing to its higher non-linearity. However, for very low pumping power as in our case, the *c* axis cleavable GaSe could not be employed in a resonant-cavity configuration due to its much higher near-IR loss. $AgGaS_2$ remains the only alternative near-IR low-loss chalcogenide material, despite a strong multi-phonon absorption peak at around 10 μm.

In this paper, we report the spectroscopic applications of a unique cw DFG spectrometer pumped by two low-power narrow-line-width ($\Delta\nu \leq 100$ kHz) near-IR diode laser systems (at $\lambda_3 \simeq 778$ nm with useful power $P_3 = 35$ mW and $\lambda_2 \sim 842$ nm with useful power $P_2 = 120$ mW), down converting $P_1 \simeq 30$ nW of useful $\lambda_1^{-1} = \lambda_3^{-1} - \lambda_2^{-1}$ radiation that is tunable in the 9- to 12-μm range by type-II (eoe) critically phase-matched DFG in $AgGaS_2$ [16, 18]. The DFG process is doubly resonant on both pump wavelengths to enhance the available pump powers. The dual-cavity resonator and the tuning procedure of the spectrometer (making use of multiple servo-loops) are described in Sect. 2. The doubly resonant design and the low output power are responsible for a noisy baseline (affected by etalon effects) of the mid-IR signal when one of the pump lasers (λ_3) is continuously tuned over 3 GHz. Unlike the standard differential noise reduction technique, we implement an analogue ratioing technique between a reference signal path and the absorbing path to cancel all etalon effects, resulting in a 10-fold increase in signal-to-noise ratio (S/N) (Sect. 3). In Sect. 4, we perform continuous Doppler scans over approximately 90 GHz of the ν_3 band of SF_6 at 10.2 μm, and the line-assignment results are compared with the prediction of pub-

✉ Fax: +33-1/43255542, E-mail: jean-jacques.zondy@obspm.fr

lished spectroscopic databases. Further attempts to observe a cavity-enhanced saturation dip on an isolated Doppler line of NH_3 failed due to the limited available power.

2 The dual-cavity spectrometer

2.1 *Experimental setup and DFG conversion efficiency*

Figure 1 shows the schematics of the final version of the DFG spectrometer. The two pump sources are made of two master/slave AlGaAs diode laser systems, Master-Oscillator/Power-Amplifier (MOPAs), tunable (by ± 5 nm) around the nominal wavelengths $\lambda_3 = 780$ nm and $\lambda_2 = 843$ nm. The master oscillators (SDL-5400 series with nominal power 50 mW) are made of extended-cavity diode lasers (ECDLs) in the Littrow cavity configuration. Injection locking of the two slave diode lasers (SDL-5400 with nominal power 50 mW at 780 nm and SDL-5420 with nominal power 150 mW at 843 nm) is performed by sending 50 μW of the master outputs via one of the side ports of the Faraday isolators located in front of each slave, yielding an injection-locking range of 3 GHz. The central wavelengths, monitored by a lambda meter (± 0.001 nm accuracy), could be tuned over the 775- to 785-nm and 839- to 848-nm ranges, for λ_3 and λ_2 respectively, so that the generated mid-IR wavelength matched $\lambda_1 = 9$–$12\,\mu$m. The injecting beam of the

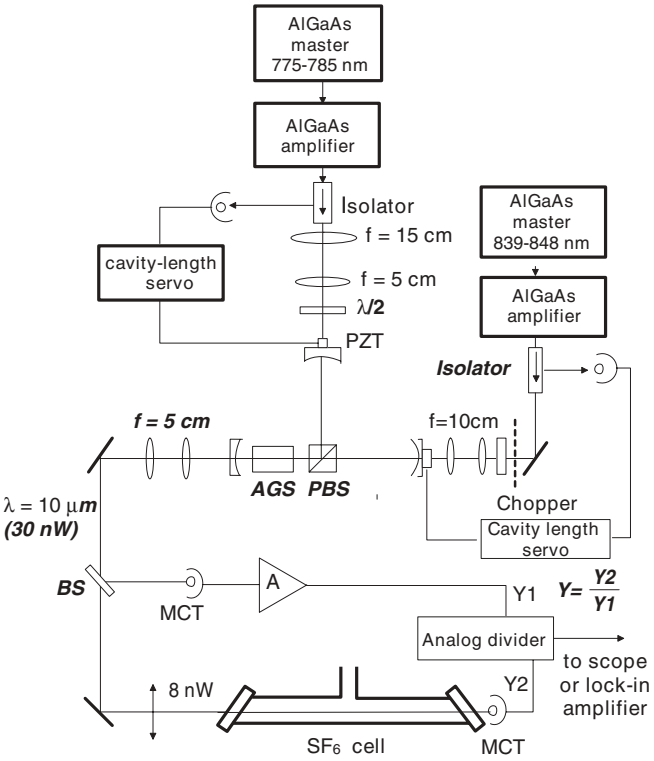

FIGURE 1 Simplified schematics of the dual-cavity DFG spectrometer setup. The two input silica mirrors have radius of curvature ROC = 70 mm and are partially transmitting in the near IR ($T_3 = 0.91$, $T_2 = 0.95$). The output ZnSe dichroic mirror (ROC = 75 mm) is highly reflecting in the near IR ($R_{2,3} > 0.99$) and highly transmissive in the 9- to 11-μm range ($T_1 = 0.9$). The physical lengths of the λ_2 arm and the λ_3 arm are respectively 110 mm and 141 mm. The pump finesses, for an average round-trip loss $a \sim 0.15$ in each arm, are $F_3 = 22$ and $F_2 = 26$, corresponding to power enhancements of $Q_3 = 3$ and $Q_2 = 5$. The maximum TEM_{00} coupling efficiencies are $\eta_3 = 75\%$ and $\eta_2 = 50\%$

λ_2 slave diode is double-passed in a 200-MHz acousto-optic modulator (AOM) for further master/slave isolation and additional fine-frequency tuning over 100 MHz by sweeping the rf drive of the AOM over 50 MHz. Single-stage Faraday isolators (−35 dB), providing imperfect (resulting in a reduced injection-locking range) but sufficient isolation from the dual-arm cavity feedback, protected the pump sources from the intense back-reflection from each arm of the linear cavity. Approximately 50% (at λ_2) and 70% (at λ_3) of the incoming powers ($P_2 = 120$ mW and $P_3 = 35$ mW) were mode matched into the dual cavity, due to non-perfect Gaussian beam profiles. Let us recall that, in a previous setup [16, 18], a λ_3 master ECDL providing 7-mW output and a commercial ECDL tapered semiconductor laser at 842 nm (SDL-8630) providing up to 350-mW output were used as pump-laser sources. This latter pump, suffering from mode-hoping tendency, was replaced with the lower-power MOPA system.

The dual-arm cavity design was chosen so as to enhance independently the power of the two pump lasers, and to relax the constraints related to the simultaneous resonance of two pump wavelengths within the same resonator (such a simultaneous resonance would be conditioned to a fortuitous resonator length). Furthermore, the two independent arms allow us to adjust the two pump waist values so as to optimise the DFG efficiency using the rigorous focused-beam DFG theory taking absorption losses, walkoff, interaction type and independent pump focusing into account [19]. The type-II (eoe) phase matching in $AgGaS_2$ ($\theta = 46°, \varphi = 0°$) ensures a maximum effective non-linear coefficient ($d_{\text{eff}}(\text{II}) = d_{36} \sin 2\theta \cos 2\varphi \simeq d_{36} = 13$ pm/V [20] instead of $d_{\text{eff}}(\text{I}) = 8$ pm/V [16, 18]). The $AgGaS_2$ crystal ($L = 15$ mm, with measured near-IR absorption loss $\alpha_{3,2} \simeq 0.02\,\text{cm}^{-1}$), was broadband anti-reflection coated in the near IR (750–900 nm). The multi-layer coatings were designed so as to reduce the Fresnel loss at λ_1. A selected low-loss (< 1% per round trip), broadband near-IR polarising cube beam splitter (PBS) allowed the coupling of the o_2 and e_3 orthogonally polarised waves in the common arm of the dual resonator. This cube replaced the lossy Glan–Thompson polariser used in the preliminary version of the spectrometer that further employed a type-I-cut crystal [16]. The major source of intra-cavity loss stemmed from the near-IR $AgGaS_2$ residual absorption, which amounted to about 6% per round trip in the standing-wave arms, hence limiting the pump-power enhancement. The two input mirrors (Fig. 1) had transmissivity factors $T_3 = 0.11$ and $T_2 = 0.4$ to optimise the impedance-matching conditions of the intra-cavity low-depletion DFG process. The measured intra-cavity power-enhancement factors in both arms were $Q_3 \simeq 3$ and $Q_2 \simeq 5$, where $Q = P^{\text{c}}/P^{\text{in}}$ is the ratio of the intra-cavity power to the mode-matched power.

For a degeneracy pump parameter $\mu = k_2/k_3$ ($k_i = 2\pi n_i/\lambda_i$) and a walkoff parameter $B = \varrho\sqrt{k_1 L}/2 = 1.6$ ($\varrho = 1.25° = 22$ mrad is the e-wave walkoff angle) the theoretical conversion efficiency $\Gamma_{\text{DFG}} = P_1/P_3P_2$ in the undepleted pump limit is [19]

$$\Gamma_{\text{DFG}} = \frac{8\omega_1^2 d_{\text{eff}}^2}{\pi\varepsilon_0 c^3 n_1 n_2 n_3} L(k_2^{-1} - k_3^{-1})^{-1} \times \exp(-\alpha_1 L)\, h_{\text{DFG}}(B, \mu). \quad (1)$$

The aperture function h_{DFG} was found to dramatically decrease as $\mu \to 1$, i.e. for deep mid-IR generation ($\omega_2 \to \omega_3$) as in our case ($\mu = 0.93$) [19]. When optimised over the focusing parameters and waist common location f_c inside the crystal ($0 \le f_c \le L$), and taking into account the three-phonon absorption peak of $AgGaS_2$ at 10 microns ($\alpha_1 = 0.5\,cm^1$), (1) yields optimal pump waist values $w_3^{opt} = 66\,\mu m$ and $w_2^{opt} = 81\,\mu m$ corresponding to $h_{DFG}(II) = 0.6592 \times 10^{-3}$ and a theoretical $\Gamma_{DFG} = 5.35\,\mu W/W^2$. Due to the strong mid-IR absorption, the optimal relative waist location from the input facet is $f = f_c/L = 0.64$. The optical path length of each arm of the dual resonator was set so as to obtain pump waist values close to the optimal ones. Furthermore, as an advantage of the folded dual cavity, the λ_3 pump e-beam axis after the coupling PBS cube was slightly laterally shifted with respect to the λ_2-beam axis (by ϱf_c) so that the two waists overlapped at the common position f_c (in a commonly shared resonator, due to focusing and walkoff, those two waists would not overlap inside the medium, resulting in a lower efficiency [19]). Both arm lengths could be servoed to the incoming pump frequency by dithering (at $f = 20\,kHz$) each of them using the piezoelectric transducer (PZT)-carrying input mirrors, followed by $1f$ demodulation of the back-reflected light exiting the side port of the isolators, and locking onto the minimum of the reflection fringe using the dispersion-shaped error signal. When one arm length was locked and the other swept, the doubly resonant mid-IR signal showed up synchronously with the scanned pump fringes, allowing an optimal alignment of the dual-arm cavity (Fig. 2). Continuous-wave operation is obtained by locking the other arm. Let us note that when both arms are locked, despite the low Q's, some slight thermo-optic self-stabilisation effect [21, 22] can be evidenced from the asymmetry of the pump resonance fringes under contracting arm length: even when the servo-loops are switched off the double-resonance condition could be passively maintained for several minutes. When the two input coupling

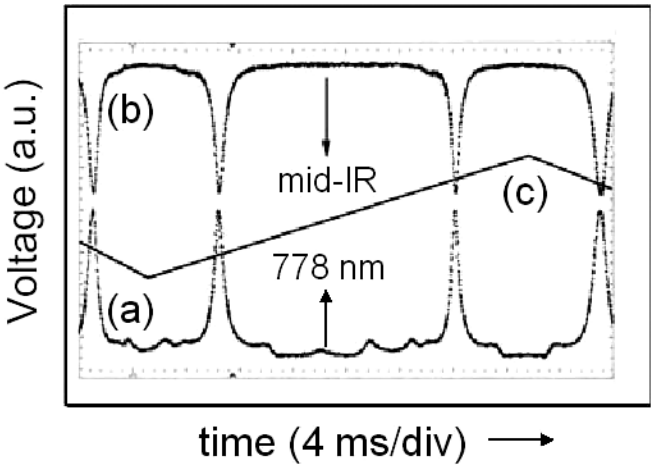

FIGURE 2 a Oscilloscope trace of the reflection-mode fringes of the λ_3 pump when the λ_2 arm is servoed. Note the fringe broadening due to thermal self-stabilisation on the last fringe corresponding to the descending slope (decreasing arm length) of the PZT voltage ramp (c). b Mid-IR transmission fringes

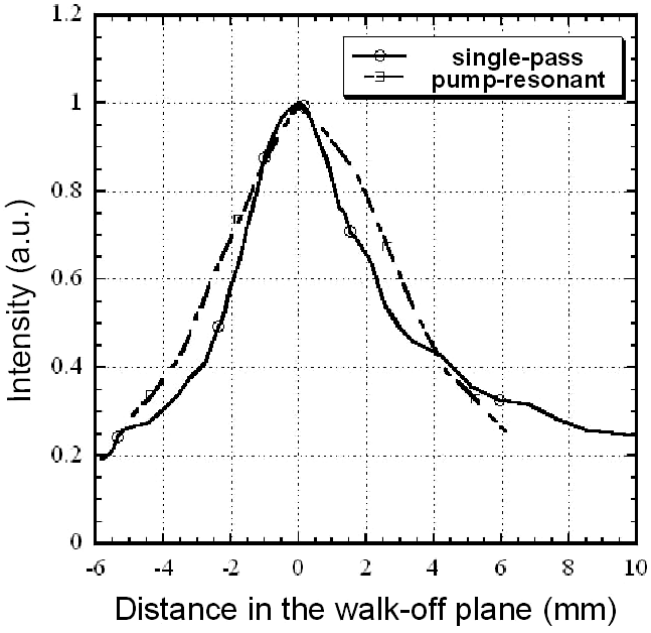

FIGURE 3 *Solid line*: section of the mid-IR beam profile in the transverse plane affected by the walkoff of the e-wave, recorded after the ZnSe output mirror under single-pass DFG. The asymmetry is due to the aperture and walkoff effects in focused-beam DFG [19]. *Dashed line*: same section, when the pump is resonating. The nearly Gaussian X-profile is due to the pump spatial filtering effect of the dual cavity, but the two-dimensional profile remains elliptical, with an ellipticity ratio of 3:1

mirrors were removed, the single-pass efficiency measured using the waists produced by the two mode-matching lenses ($w_3 = 75\,\mu m$ and $w_2 = 96\,\mu m$) was $\Gamma_{exp} = 2.86\,\mu W/W^2$. The discrepancy factor of 1.87 with the above theoretical value can be attributed to the non-optimal waists and to the non-Gaussian feature of the pump beams under single-pass DFG. In addition, due to the aberrations of the highly elliptical profile (ellipticity ratio 3 : 1) of the mid-IR radiation detected after the ZnSe output coupler (Fig. 3), not all the power could be focused onto the 300-μm diameter of a cryogenically cooled HgCdTe (MCT) photovoltaic detector (detectivity $D^* = 4.5 \times 10^{10}\,cm\,Hz^{1/2}\,W^{-1}$ at 11 μm). The maximum mid-IR power exiting the dual cavity at maximum available pump powers just before the input mirrors ($P_3^m = 35\,mW$ and $P_2^m = 120\,mW$) was limited to $P_1^m = 50\,nW$. Considering that only 70% ($P_3^{eff} = 24\,mW$) and 50% ($P_2^{eff} = 60\,mW$) of the incident pump powers are mode matched to both arms, the mid-IR power corresponded to intra-cavity pump powers $P_3^c = 105\,mW$ and $P_2^c = 315\,mW$ (evaluated from $\Gamma_{exp} = P_1^m / P_3^c P_2^c$), consistent with the independently measured Q's. The available mid-IR power is far from the targeted 1-μW level, but scales favourably in comparison with the reported single-pass long-wavelength DFG experiments at the same available pump power [8, 10, 15].

3 Mid-IR baseline noise cancellation

With the baseline shown in curve (a) of Fig. 4, it would be difficult to discriminate between artefact and true spectroscopic lines, especially for the dense ν_3-band rovibrational transitions of SF_6 in the 10-micron range. An example of noisy SF_6 spectra recorded with the direct output of

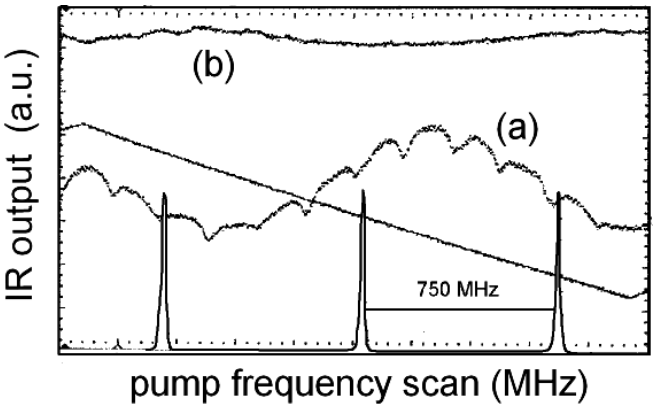

FIGURE 4 Continuous scan of the DFG spectrometer over 2.5 GHz. The *bottom fringe system* is the pump transmission as analysed by the near-IR CFP, when the λ_3 pump is frequency tuned during one descending slope of the triangular voltage ramp (shown). Curve (a) shows the 10.2-μm mid-IR baseline. Curve (b) shows the mid-IR baseline after noise and etalon effect cancellation. The improvement in S/N ratio from (a) to (b) is 10

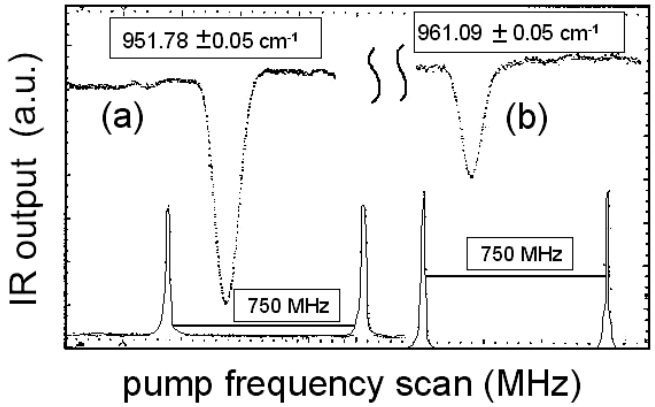

FIGURE 5 Doppler spectra of the $aR(0,0)$ line (a) and the $sQ(10,9)$ line (b) of NH_3 in the 10.5-μm range. The relative intensity of both lines is preserved. The *lower fringes* show one free spectral range of the near-IR CFP monitoring the pump-frequency scan

the spectrometer can be found in [24]. To cancel the spurious noise in DFG spectrometers, a standard technique consists in splitting the IR signal (using a 50/50 beam splitter) into a reference path [with intensity $I_R = I_0(\nu)$] and a path comprising the absorption cell [$I_{abs} = I_0(\nu)\exp -\alpha(\nu)l$], and to obtain the analogue voltage difference between the balanced outputs of both detectors,

$$I_d(\nu) = I_{abs} - I_R = I_0(\nu)\,\{\exp -\alpha(\nu)l - 1\}\,, \qquad (2)$$

where l is the cell length and $\alpha(\nu)$ the absorption line shape. Far from an absorption line ($\alpha(\nu) \equiv 0$), the background noise is indeed cancelled and the baseline translated to zero voltage, where the detection sensitivity of weak lines is the highest. However, in the vicinity of a line, the noisy baseline $I_0(\nu)$ will alter the line shape when the scale of perturbation is of the order of the line width. Implementing this difference-based balanced detection technique partially cancelled the slow modulation in Fig. 4, curve (a) but failed to suppress the fast one. A better strategy was to obtain the ratio of the two photodetector signals by use of an analogue voltage divider (Analog Devices AD734), providing a transfer function $Y = Y_1/Y_2 \propto \alpha(\nu)l$ that does not alter the line shape (see lower part of Fig. 1). The resulting baseline is shown in Fig. 4, curve (b), where all etalon effects are practically cancelled, and the intrinsic detector noise reduced, leading to a 10 times improvement in S/N ratio. We have tested this noise-cancellation scheme by recording isolated spectral lines of ammonia (NH_3) in the 10.5-μm range, belonging to the ν_2 combination band [25, 26]. Only $P_1 = 8$–12 nW of power, focused to a waist of 300 μm ($I_1 = 2.8$–$3.5\ \mu W/cm^2$), was available at the entrance of the Brewster cell ($l = 20$ cm) filled with 100 mTorr (13.33 Pa) of pure NH_3. A direct single sweep of the spectrometer, without any lock-in-detection apparatus, led to the spectra shown in Fig. 5. The pump wavelengths were set to $\lambda_3 = 782.479$ nm and $\lambda_2 = 845.443$ nm [$\lambda_1 = 10.50664$ μm, $\sigma_1 = 951.778\,(\pm 0.033)\,cm^{-1}$] for the case of the $aR(0,0)$ line labelled (a) with assigned wavenumber $951.77631\,cm^{-1}$ [25] and dipole moment $\mu = 0.116$ D [26]. The second weaker line (b), corresponding to the assigned transition $sQ(10,9)$ ($961.08589\,cm^{-1}$, $\mu = 0.0396$ D [25, 26]), was recorded at $\lambda_3 = 783.360$ nm and $\lambda_2 = 847.140$ nm ($\lambda_1 = 10.40469$ μm, $\sigma_1 = 961.105\ (\pm 0.033)\,cm^{-1}$). According to the Confocal Fabry–Pérot calibration, the FWHM Doppler width of both lines is $\Gamma_D \simeq 80$ MHz.

In a second step, we have tried to perform sub-Doppler spectroscopy of the most intense ro-vibrational transition $aR(0,0)$, despite the 8-nW power level available on path Y2 (Fig. 1) but relying on the large dipole moment of spherical molecules in the 10-micrometre range. To enhance the available power, the Brewster cell was placed inside a resonator made of two curved (ROC = 1 m, $T = 0.9$) CO_2-laser output couplers. The large ROC of the mirrors prevented us from reducing further the beam waist and the mirror spacing was set to 40 cm to mode match the 300-μm waist of the mid-IR focused beam. The elliptical beam shape was circularised prior to focusing using two ZnSe anamorphic prism pairs, so that less than 5 nW could be coupled into the resonator (finesse $F_1 \simeq 20$). One of the CO_2-laser mirrors was driven by a PZT ceramic to lock the Fabry–Perot resonator to the sweeping mid-IR frequency. This servo was implemented in the following way. The frequency of the 50-μW beam injecting the λ_2 slave amplifier was modulated at $f = 22$ kHz via the double-passed AOM with 200-MHz nominal operating rf drive. The subsequent frequency modulation (FM) patterned on the mid-IR light was converted into amplitude modulation (AM) by the discriminating fringe slope of the saturation cavity, and part of the transmitted amplitude modulation was $1f$ demodulated by a lock-in amplifier and used to lock the length of the Fabry–Perot to the top of one mid-IR fringe. The saturation cavity followed the spectrometer scan on both slopes of the triangular voltage ramp. Figure 6a displays the $aR(0,0)$ Doppler profile observed in transmission of the saturation cavity, and no apparent Lamb dip could unfortunately be observed at the top of the Doppler profile.

To enhance the detection sensitivity, we have further attempted a $1f$ lock-in amplifier detection of the Doppler profile, in order to detect an eventual dip on the line profile derivative near the zero-voltage crossing point. The FM-to-AM lock of the saturation cavity was replaced with a side-of-fringe locking technique, the locking point on the fringe

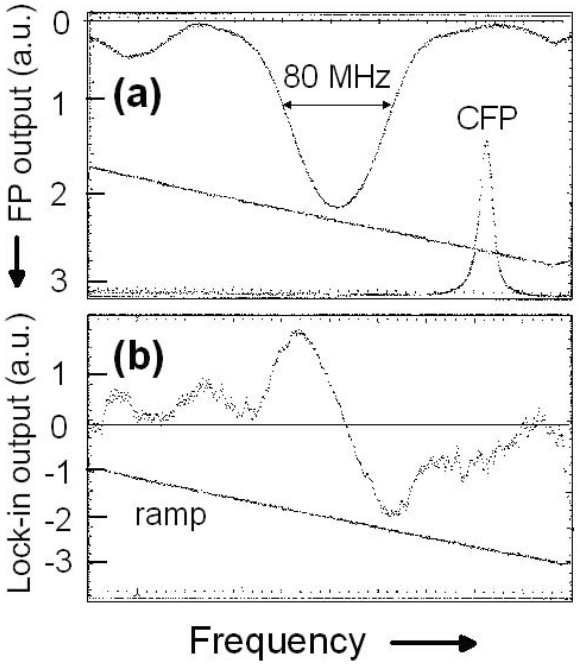

FIGURE 6 Curve **a**: Doppler profile of the $aR(0,0)$ transition of NH_3 recorded in transmission of the mid-IR Fabry–Perot cavity. Curve **b**: $1f$ demodulated derivative of the Doppler profile (see text)

being controlled by a reference bias voltage. The amplitude of the 22-kHz frequency modulation was reduced to 1–2 MHz (the presumed value of the homogeneous line width), and the transmitted amplitude-modulated signal sent to the lock-in amplifier. The resulting spectrum is shown in Fig. 6b, but again no evidence of a saturation dip was found, even by varying the modulation depth. The saturation intensity in the transit-time-limited regime can be estimated as [13]

$$I_S = \frac{\varepsilon_0 c \hbar^2 \Gamma_\perp^2}{2\mu^2}, \tag{3}$$

where $\Gamma_\perp$ is the homogeneous line width. Setting $\Gamma_\perp = 1\,\text{MHz}$ yields $I_S = 40\,\mu\text{W/cm}^2$. Estimating the intra-cavity power to be $P_1^c \simeq 15\,\text{nW}$ yields an intensity of $I_1^c \simeq 5\,\mu\text{W/cm}^2 \ll I_S$. We believe that the too-low available power is responsible for the failure of the saturation spectroscopy experiment, given the large-enough S/N ratio of the detection apparatus as evidenced from Fig. 6. In [14], a laser spectrometer based on single-pass DFG of a Nd–YAG laser and a 850-nm diode laser (delivering 12-μW output at $\lambda_1 = 4.3\,\mu\text{m}$) has been used to observe a good-contrast Lamb dip in CO vapour. Improving the DFG conversion efficiency to $P_1 \geq 1\,\mu\text{W}$ would suffice for our purpose, either by replacing the pump slave lasers with 0.5-W tapered power amplifiers or by reducing further the dual-cavity losses.

4 Doppler spectroscopy of SF_6

We demonstrated the usefulness of the dual-cavity spectrometer for wide-range continuous scans ($\Delta\sigma \simeq 3\,\text{cm}^{-1}$) in the 10.2-micrometre range using only 12 nW of power by recording the Doppler spectra of part of the ν_3 band of SF_6. A similar low-power level was recently used to record Doppler lines of SO_2 over about $1\,\text{cm}^{-1}$ [27]. Figure 7 shows the continuous scans of the P branch from $P(15)$ to $P(23)$, and Fig. 8 the scans of the R branch from $R(9)$ to $R(17)$. The tick marks above the the recorded spectra correspond to P and R lines as calculated (lower spectra) from the HAWKS software of the HITRAN database [26]. In spite of the dense contamination by additional combination-band lines, the P- and R-line assignments were facilitated by the rather high mid-IR accuracy ($\simeq 1\,\text{GHz}$) provided by the lambda meter, and the availability of theoretical data on the frequencies and line intensity ratios within each substructure. Such an easy assignment would not have been possible without the baseline noise cancellation. The precise frequency knowledge of the lines reported in Figs. 7 and 8 would help in improving the molecular potential of SF_6 or any other species (see Sect. 5). If one compares the wavenumber range explored in both spectra ($946.5–949\,\text{cm}^{-1}$) to the wavenumber range of lasing CO_2 lines as published by Freed et al. [3] (including all isotopes), one realises that such a target spectral range is not covered by the CO_2 laser. Furthermore, in a spectrally dense region such as that investigated here, it is important to have extended continuous tuning capability to allow an easy assignment of the spectroscopic lines. Only a DFG source can provide such a capability.

5 Conclusions and prospects

We have demonstrated an original, compact, low-power DFG spectrometer that is capable of performing high-resolution spectroscopy of molecular species in the deep mid IR. The spectrometer is based on cw, low-power ($P_3 P_2 = 42 \times 10^{-4}\,\text{W}^2$) near-IR diode lasers, and uses a dual-arm cavity to realise a doubly resonant DFG in silver thiogallate crystal. Continuous frequency tuning by steps of 3 GHz over $3\,\text{cm}^{-1}$ has been demonstrated without dual-cavity realignment, using several electronic servo-loops. The continuous tuning range can be further extended to a few tens of GHz with an additional current servo-loop on one of the slave diode pump lasers. A single angle-tuned type-II-cut $AgGaS_2$ crystal can cover the 9- to 12-μm range. We have also developed a noise-cancellation technique, based on analogue signal ratioing, to cancel the noisy baseline of low-power DFG spectrometers and improve the S/N ratio. The performance of the dual-cavity spectrometer has been demonstrated by recording spectra of the ν_3 band of SF_6 over approximately $3\,\text{cm}^{-1}$.

Room is left for scaling up the low DFG power ($P_1 \simeq 50\,\text{nW}$), by selecting an extremely low-loss crystal or using a shorter $AgGaS_2$ crystal minimising the round-trip near-IR loss and mid-IR absorption, and improving the pump mode-matching efficiency. To reach the microwatt power level with the present setup, an enhancement of the Q-factor of each arm of the resonator by ~ 5 is required. One other possible improvement in conversion efficiency, apart from scaling up the pump-laser power or reducing further the intra-cavity loss, is to use a monolithic walkoff-compensating periodic $AgGaS_2$ structure composed of $2N$ thin optically contacted plates, to cancel the focused-beam aperture effect due to the rather large walkoff angle [18, 31]. Such a periodic structure made from KTP with $2N = 10$, namely the $2N$-OCWOC structure,

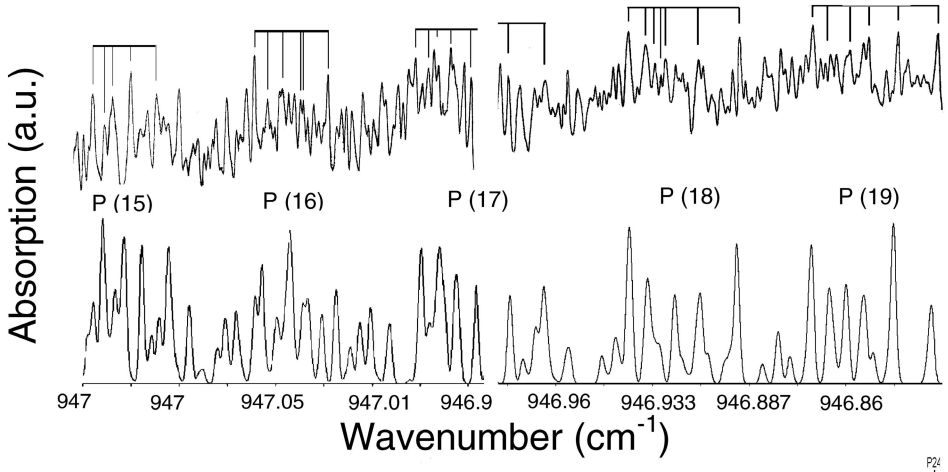

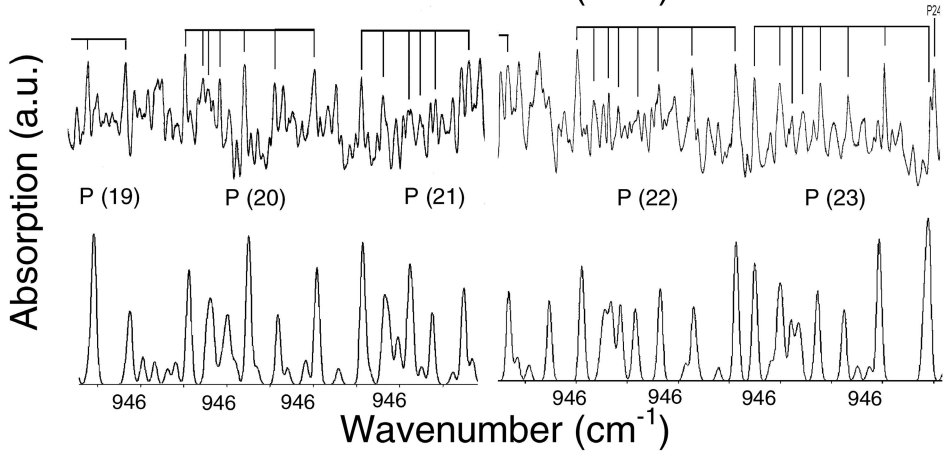

FIGURE 7 *Upper traces*: Doppler spectra of P(15) to P(23) lines of the ν_3 band of SF_6, recorded with 12-nW output from the DFG spectrometer using the noise ratioing cancellation technique. The cell pressure was 50 mTorr. *Lower curves*: calculated P-line spectra based on HITRAN96 data, which match the *tick-marked lines* on the *upper spectra*. Note that many additional combination lines not given in the database show up in the experimental recordings

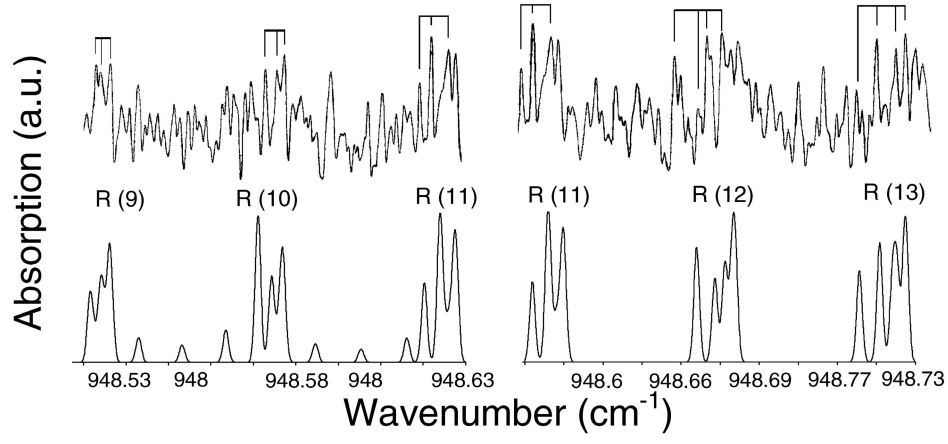

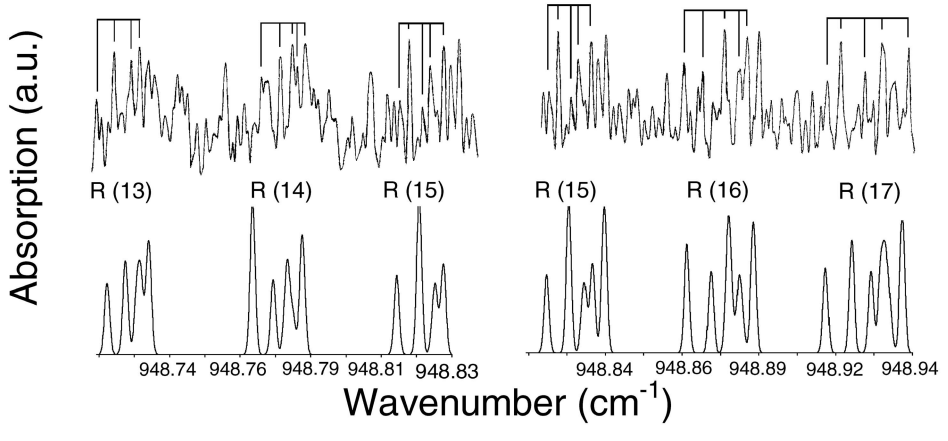

FIGURE 8 Same as in Fig. 7, except that the recordings are for the *R* branch of the ν_3 band of SF_6

has recently been shown to enhance the efficiency of single-pass type-II second-harmonic generation by a factor 22 as compared with the efficiency of a single bulk non-walkoff-compensated KTP crystal [32]. The same kind of enhancement is expected in deep mid-IR down-conversion processes.

The use of cw pump sources can potentially provide further ultra-high resolution, by preliminarily locking both master lasers to the same high-finesse resonator: in such a scheme, in addition to the benefit of even narrower pump line widths on the sub-kHz level, the residual common-mode frequency noise of the lasers is automatically rejected by the down-conversion process, with an ultimate mid-IR line width on the Hz level, as in [1]. In such an ultra-high-resolution scheme, an additional λ_3 ECDL diode laser offset phase locked to the cavity-stabilised laser would be required for tuning purposes. With the recent breakthrough brought by mode-locked titanium–sapphire (Ti : Sa) femtosecond-laser-based frequency chains that can reach the Hertz-level measurement accuracy [28], ultra-high-resolution spectroscopy of molecules in the deep mid-IR range becomes possible with such a device since, for measuring the mid-IR frequencies, it suffices to measure the frequency difference between the near-IR pump lasers using the stabilised frequency comb of the mode-locked laser [29]. Although the number of cascaded servo-loops necessary for the frequency scan precludes the use of such a spectrometer for in situ environmental monitoring, in laboratory applications it would advantageously replace a bulky high-resolution Fourier-transform infrared spectrometer setup. To that purpose, the diode-pump systems can be replaced, at a higher cost, with two 1-W frequency-stabilised Ti : Sa lasers, without the further need of a dual resonator.

As an alternative frequency-metrology application, locking the dual-cavity spectrometer to a well-behaved saturation dip would provide an ultra-stable, tunable IR frequency standard not relying on a CO_2-laser coincidence line [30]. Although we could not perform saturation spectroscopy with the present available power, scaling up the DFG power to 1-μW level and performing the sub-Doppler spectroscopy within a high-finesse resonator is realistic, as demonstrated here. The metrological performance in fractional frequency stability (better than 10^{-14}) and accuracy of unaccessible OsO_4 isolated hyperfine transitions in the 30-THz spectral range can be investigated using such a tunable deep mid-IR source.

ACKNOWLEDGEMENTS This work has benefited from a partial funding from a European Union grant (INCO-Copernicus programme, Contract No. IC15-CT98-0814). The authors acknowledge Dr. A. Clairon (BNM-SYRTE) for the idea of the analogue ratioing noise cancellation technique, and Dr. O. Acef for providing the mid-IR detection apparatus and the SF_6 spectroscopic line database.

REFERENCES

1 C. Salomon, C. Bréant, A. van Lerberghe, G. Camy, C.J. Bordé: Appl. Phys. B **29**, 153 (1982)
2 E.N. Bazarov, G.A. Gerasimov, V.P. Gubin, N.I. Starostin, V.V. Fomin: Sov. J. Quantum Electron. **14**, 195 (1984)
3 C. Freed, L.C. Bradley, R.G. O'Donnell: IEEE J. Quantum Electron. **QE-16**, 1195 (1980)
4 F. Capasso, C. Gmachl, R. Paiella, A. Tredicucci, A.L. Hutchinson, D.L. Sivco, J.N. Baillargeon, A.Y. Cho, H.C. Liu: IEEE J. Sel. Top. Quantum Electron. **6**, 931 (2000)
5 K. Ohtani, H. Ohno: Appl. Phys. Lett. **82**, 1003 (2003)
6 D. Hofstetter, M. Beck, T. Aellen, J. Faist, U. Oesterle, M. Ilegems, E. Gini, H. Melchior: Appl. Phys. Lett. **78**, 1964 (2001)
7 P. Canarelli, Z. Benko, R.F. Curl, F.K. Tittel: J. Opt. Soc. Am. B **9**, 197 (1992)
8 W.C. Eckoff, R.S. Putnam, S. Wang, R.F. Curl, F.K. Tittel: Appl. Phys. B **63**, 437 (1996)
9 U. Simon, C.E. Miller, C.C. Bradley, R.G. Hulet, R.F. Curl, F.K. Tittel: Opt. Lett. **18**, 1062 (1993)
10 V. Petrov, C. Rempel, K.P. Stolberg, W. Schade: Appl. Opt. **37**, 4925 (1998)
11 K.P. Petrov, R.F. Curl, F.K. Tittel, L. Goldberg: Opt. Lett. **21**, 1451 (1996)
12 B. Sumpf, D. Rehle, T. Kelz, H.-D. Kronfeldt: Appl. Phys. B **67**, 369 (1998)
13 D. Mazzotti, P. De Natale, G. Giusfredi, C. Fort, J.A. Mitchell, L. Hollberg: Opt. Lett. **25**, 350 (2000)
14 S. Borri, P. Cancio, P. De Natale, G. Giusfredi, D. Mazzotti, F. Tamassia: Appl. Phys. B **76**, 473 (2003)
15 W. Chen, G. Mouret, D. Boucher: Appl. Phys. B **67**, 375 (1998)
16 D. Lee, T. Kaing, J.-J. Zondy: Appl. Phys. B **67**, 363 (1998)
17 A.A. Kosterev, R.F. Curl, F.K. Tittel, R. Köhler, C. Gmachl, F. Capasso, D.L. Sivco, A.Y. Cho: Appl. Opt. **41**, 573 (2002)
18 T. Kaing, J.-J. Zondy, A.P. Yelisseyev, S.I. Lobanov, L.I. Isaenko: IEEE Trans. Instrum. Meas. **48**, 592 (1999)
19 J.-J. Zondy: Opt. Commun. **149**, 181 (1998)
20 J.-J. Zondy, D. Touahri, O. Acef: J. Opt. Soc. Am. B **14**, 2481 (1997)
21 A. Douillet, J.-J. Zondy, A. Yelisseyev, S. Lobanov, L. Isaenko: J. Opt. Soc. Am. B **16**, 1481 (1999)
22 T. Kaing: Ph.D. dissertation, U.F.R. Scientifique d'Orsay, Université de Paris XI (1999)
23 J.-J. Zondy, D. Touahri: J. Opt. Soc. Am. B **14**, 1331 (1997)
24 T. Kaing, J.-J. Zondy, A. Yelisseyev, S. Lobanov, L. Isaenko: IEEE Trans. Ultrason. Ferroelectr. Freq. Control **47**, 506 (2000)
25 G. Guelachvili, K.N. Rao: *Handbook of Infrared Standards* (Academic, Orlando 1986) pp. 147–149 (1986)
26 L.S. Rothman, C.P. Rinsland, A. Goldman, S.T. Massie, D.P. Edwards, J.M. Flaud, A. Perrin, C. Camy-Peyret, V. Dana, J.Y. Mandin, J. Schroeder, A. McCann, R.R. Gamache, R.B. Watson, K. Yoshin, K.V. Chance, K.W. Jucks, L.R. Brown, V. Nemtchinov, P. Varanasi: J. Quantum Spectrosc. Radiat. Transfer **60**, 665 (1996) [software available at http://cfa-www.harvard.edu/HITRAN]
27 J. Henningsen, J. Hald: Appl. Phys. B **76**, 441 (2003)
28 R. Holzwarth, T. Udem, T.W. Hänsch, J.C. Knight, W.J. Wadsworth, P.S.J. Russell: Phys. Rev. Lett. **85**, 2264 (2000)
29 S.A. Diddams, D.J. Jones, L.S. Ma, S.T. Cundiff, J.L. Hall: Opt. Lett. **25**, 186 (2000)
30 O. Acef: Opt. Commun. **134**, 479 (1997)
31 J.-J. Zondy, C. Bonnin, D. Lupinski: J. Opt. Soc. Am. B **20**, 1675 (2003)
32 J.-J. Zondy, D. Kolker, Ch. Bonnin, D. Lupinski: J. Opt. Soc. Am. B **20**, 1695 (2003)